HHS Public Access

Author manuscript

Hippocampus. Author manuscript; available in PMC 2021 November 04.

Published in final edited form as:

Hippocampus. 2021 November ; 31(11): 1215–1232. doi:10.1002/hipo.23386.

Direct Synaptic Excitation between Hilar Mossy Cells Revealed with a Targeted Voltage Sensor

Yihe Ma,
Department of Neuroscience, University of Wisconsin – Madison, WI 53705

Peter O. Bayguinov,
Washington University Center for Cellular Imaging, Washington University School of Medicine, St Louis MO 63110

Shane M. McMahon,
Department of Neuroscience, University of Wisconsin – Madison, WI 53705

Helen E. Scharfman,
New York University Langone Health and the Nathan Kline Institute for Psychiatric Research, Orangeburg, NJ 10962

Meyer B. Jackson
Department of Neuroscience, University of Wisconsin – Madison, WI 53705

Abstract

The dentate gyrus not only gates the flow of information into the hippocampus, it also integrates and processes this information. Mossy cells (MCs) are a major type of excitatory neuron strategically located in the hilus of the dentate gyrus where they can contribute to this processing through networks of synapses with inhibitory neurons and dentate granule cells. Some prior work has suggested that MCs can form excitatory synapses with other MCs, but the role of these synapses in the network activity of the dentate gyrus has received little attention. Here we investigated synaptic inputs to MCs in mouse hippocampal slices using a genetically-encoded hybrid voltage sensor (hVOS) targeted to MCs by Cre-lox technology. This enabled optical recording of voltage changes from multiple MCs simultaneously. Stimulating granule cells and CA3 pyramidal cells activated well established inputs to MCs and elicited synaptic responses as expected. However, the weak blockade of MC responses to granule cell layer stimulation by DCG-IV raised the possibility of another source of excitation. To evaluate synapses between MCs as this source, single MCs were stimulated focally. Stimulation of one MC above its action potential threshold evoked depolarizing responses in neighboring MCs that depended on glutamate receptors. Short latency responses of MCs to other MCs did not depend on release from granule cell axons. However, granule cells did contribute to the longer latency responses of MCs to stimulation of other MCs. Thus, MCs transmit their activity to other MCs both through direct synaptic coupling and through polysynaptic coupling with dentate granule cells. MC-MC synapses can redistribute information entering the dentate gyrus and thus shape and modulate the electrical

Correspondence: Meyer B. Jackson, Department of Neuroscience, University of Wisconsin, Madison, WI, Meyer.Jackson@Wisc.edu.

activity underlying hippocampal functions such as navigation and memory, as well as excessive excitation during seizures.

Keywords

Dentate gyrus; Hilus; Excitatory synapse; Glutamate receptors; Voltage imaging

Introduction

The mossy cell (MC), so named for its characteristic thorny excrescences (Amaral, 1978), resides in the hilar region of the dentate gyrus. These glutamatergic neurons receive inputs from various types of hippocampal neurons, and project both locally within the dentate gyrus as well as distally to the ipsilateral and contralateral hippocampus (Amaral, Scharfman, & Lavenex, 2007). Dentate granule cells (GCs) provide the primary excitatory drive to MCs. MCs in turn provide reciprocal excitation back to GCs, and excite GABAergic interneurons as well. Their strategic location in the hilus allows MCs to modify how the dentate gyrus processes information (Buckmaster & Schwartzkroin, 1994; Lisman, 1999; Morgan, Santhakumar, & Soltesz, 2007; Myers & Scharfman, 2009, 2011; Santhakumar et al., 2000), and to control the generation of abnormal seizure activity (Botterill et al., 2019; Bui et al., 2018; Ratzliff, Santhakumar, Howard, & Soltesz, 2002; Santhakumar et al., 2000; Scharfman, 2016; Sloviter, 1994). However, the roles MCs in these functions remain elusive. The limited knowledge of MC properties and circuitry has impeded efforts to establish their contributions to hippocampal circuit activity and function (Henze & Buzsaki, 2007; Scharfman, 2016).

The dendrites of MCs mostly reside in the hilus around their somata, and only occasionally extend into the molecular layer (Blackstad et al., 2016; Scharfman, 1991). GC axons, commonly referred to as mossy fibers, provide a major input to MCs, but semilunar GCs (Larimer & Strowbridge, 2010; Williams, Larimer, Gao, & Strowbridge, 2007), CA3 pyramidal cells, cortical neurons, and GABAergic interneurons also innervate MCs (Amaral et al., 2007; Azevedo et al., 2019; Jinde, Zsiros, & Nakazawa, 2013; Scharfman, 2018; Sun, Grieco, Holmes, & Xu, 2017). MC axons project densely to the inner molecular layer and innervate proximal GC dendrites (Buckmaster, Wenzel, Kunkel, & Schwartzkroin, 1996; Frotscher, Seress, Schwerdtfeger, & Buhl, 1991; Ribak, Seress, & Amaral, 1985), but they also occasionally enter the middle and outer molecular layers (Buckmaster, Strowbridge, Kunkel, Schmiege, & Schwartzkroin, 1992) especially in ventral DG (Botterill et al., 2021; C.R. Houser, Peng, Wei, Huang, & Mody, 2021). MC axons collateralize in the hilus close to their somata (Buckmaster et al., 1996; Ribak et al., 1985; Scharfman & Schwartzkroin, 1988), forming synapses mostly on dendritic shafts but also on somata and dendritic spines of other hilar neurons (Buckmaster et al., 1996). Voltage imaging and electrophysiological recording have shown that MCs excite GCs directly (Chancey, Poulsen, Wadiche, & Overstreet-Wadiche, 2014; Jackson & Scharfman, 1996; Scharfman, 1995; Scharfman, Kunkel, & Schwartzkroin, 1990), and inhibit GCs disynaptically via GABAergic interneurons (Bui et al., 2018; Sloviter, 1994). MC loss is associated with epilepsy (Ratzliff et al., 2002; Scharfman, 2016; Sloviter, 1994), increased anxiety, and impaired contextual

discrimination, and MC activity is necessary for spatial memory encoding (Bui et al., 2018; Jinde et al., 2012). Inhibiting and exciting MCs also has diverse behavioral effects including contextual fear conditioning and anxiety (Botterill et al., 2021). MCs play an important role in coordinating local and distal hippocampal circuits, and possibly in the integration of inputs from other brain regions (Azevedo et al., 2019).

The many functions of MCs are generally attributed to their synaptic inputs to and from GCs and inhibitory interneurons. However, there is evidence that MCs synapse with one another. Viral tracing supports the existence of such synapses (Sun et al., 2017), and photorelease of glutamate in the hilus activates MCs (Shi, Grieco, Holmes, & Xu, 2019). Recording from multiple MCs has proven difficult, but rare instances of synaptic coupling between pairs of MCs have been reported (Larimer & Strowbridge, 2008). Recent advances in targeting MCs genetically (Gangarossa et al., 2012; Jinde et al., 2012) have created exciting new opportunities to investigate MC physiology. Here we used a Cre-lox strategy to target an enhanced genetically-encoded hybrid voltage sensor (hVOS) (Bayguinov, Ma, Gao, Zhao, & Jackson, 2017; Chanda et al., 2005), and image electrical activity from multiple MCs simultaneously. Stimulating the established synaptic inputs from GCs and CA3 pyramidal cells elicited responses in MCs. Furthermore, focal stimulation of single MCs elicited synaptic responses in neighboring MCs. These experiments reveal an extensive network of MCs connected to one another by excitatory synapses. Direct synaptic connections between MCs represent a new element of circuitry in the dentate gyrus, with the potential to contribute broadly to hippocampal function.

Materials and Methods

All animal procedures were approved by the Animal Care and Use Committee of the University of Wisconsin School of Medicine and Public Health. Two different Cre drivers, purchased from the Jackson Laboratory, were used to target mossy cells: calbindin 2 (B6(Cg)-Calb2$^{tm2.1(cre/ERT2)Zjh}$/J, JAX 013730) and calcitonin receptor-like receptor (C57BL/6N-Tg(CalCrl,cre)4688Nkza/J, JAX 023014). The hVOS 1.5 probe (Wang, Zhang, Chanda, & Jackson, 2010) was targeted to MCs by crossing these two Cre drivers with the Ai35-hVOS Cre reporter described previously from this laboratory (Bayguinov et al., 2017). Female Cre reporter mice were bred with male Cre driver mice, generating double-transgenics referred to as hVOS::CalB2 and hVOS::CalCrl. Genotyping of offspring confirmed the presence of hVOS 1.5 and Cre recombinase.

Because the calbindin 2 Cre driver is coupled to estrogen receptor activation, hVOS::CalB2 mice were injected intraperitoneally 5 times on consecutive days with 100–160 mg/kg tamoxifen. This regimen has been shown to optimize recombination while minimizing lethality (Lagace et al., 2007). Tamoxifen was dissolved at 40 mg/ml in 10% EtOH mixed with 90% sunflower seed oil by 2-hour sonication or overnight nutation, and stored at 4 °C in the dark for up to one week. Animals were injected at 4–6 weeks old, and used for experiments 7–10 days following the last injection.

Brain slice preparation

Hippocampal slices were prepared from 4–10 week old mice of either sex. Animals were anesthetized by isoflurane inhalation and euthanized. The mouse was decapitated, the brain removed and immersed for 5 min in ice-cold cutting solution (in mM: 125 NaCl, 4 KCl, 1.25 NaH_2PO_4, 26 $NaHCO_3$, 6 $MgSO_4$, 1 $CaCl_2$, and 10 glucose bubbled with 5% CO_2–95% O_2), and then mounted in a cutting chamber. Horizontal slices from the ventral half of the hippocampus were cut with a Leica VT1200 tissue slicer at 350–400 μm and allowed to recover for 45–60 minutes in artificial cerebrospinal fluid (aCSF; in mM, 125 NaCl, 4 KCl, 1.25 NaH_2PO_4, 26 $NaHCO_3$, 1.3 $MgSO_4$, 2.5 $CaCl_2$, and 10 glucose) containing 4 μM dipicrylamine (DPA, City Chemical LLC) at room temperature.

Voltage imaging

Voltage imaging was conducted with an Olympus BX51 microscope equipped with a 29-W, 435-nm LED light source (Prizmatix), a cyan fluorescent protein (CFP) filter set, and an Olympus XLUMPlanFl 20X objective (NA = 1.0) or Olympus LUMPlanFl 60X objective (NA = 0.90). Images were acquired with a CCD-SMQ camera (Redshirt Imaging, now SciMeasure) at 2000 kHz with 80×80 resolution. The computer program Neuroplex provided by Redshirt Imaging with their camera controlled the timing of illumination, stimulation, and performed data acquisition. The computer program PhotoZ (Chang, 2006) was also used for imaging experiments after it was adapted for use with the CCD-SMQ camera. hVOS images were acquired as averages of from 5 to 20 trials at 5–15 s intervals. Images were directed to a higher resolution camera with a sliding mirror for DIC images.

During experiments brain slices were perfused with 95% O_2/5% CO_2-bubbled aCSF containing 4 μM DPA at room temperature. Voltage-dependent movement of DPA within the membrane modulates a FRET interaction with the membrane tethered hVOS probe to render a fluorescence signal that reports voltage changes (Chanda et al., 2005). Stimulus intensity was initially set at 200 μA based on prior studies in which stimulus was varied systematically (Bayguinov, Ghitani, Jackson, & Basso, 2015). Stimulus current was decreased in 25–50 μA intervals if directly evoked short-latency optical signals were present, or increased if responses to 200 μA were unclear. For the experiments of Figs. 2–3 the outer molecular layer (OML) simulation current was always 200 μA, and for GCL stimulation the current was 200 ± 58 μA (mean ± SD).

To stimulate slices extracellularly, 0.18-msec current pulses were applied with a model A365 stimulus isolator (World Precision Instruments) through aCSF-filled glass electrodes (King Precision Glass) with 5–10 μm openings. Single MCs were stimulated focally using theta capillary glass electrodes (King Precision Glass) with 2–3 μm openings (Cabezas & Buno, 2006). Stimulus current was varied to find the spike threshold of the stimulated cell. A micromanipulator was used to position stimulating electrodes under visual control with IR-DIC or gradient contrast optics to gently touch a selected cell with the electrode tip. The microscope stage and micromanipulator were mounted on a vibration isolation table and the microscope mounted on a translation stage so that the field of view could be adjusted after the stimulating electrode was positioned.

For drug application, we first established baselines for ~15 min and then perfused with aCSF containing drug (1 μM DCG-IV, Tocris or 10 μM NBQX, Sigma or 1 mM kynurenic acid, Alfa Aesar) for 10–20 min. Recovery was tested ~30 min after return to control aCSF.

Morphology

Brightfield epifluorescence images were taken in conjunction with imaging experiments using an IR-1000 (DAGE-MTI) or a Kiralux (Thorlabs) camera on the Olympus BX51 microscope used for hVOS experiments. For two-photon microscopy, acute brain slices or slices after immunohistochemistry staining were imaged with an Olympus BX61 microscope equipped with an Ultima scanning system (Bruker Corporation) illuminated by a Chameleon Ti:Sapphire laser (Coherent). Images were analyzed and processed in ImageJ (NIH).

Following experiments, selected slices were drop fixed in 4% paraformaldehyde (PFA), stored in 0.1 M phosphate buffer (pH 7.4) and then imaged. To amplify probe fluorescence, immunohistochemistry was performed in slices from hVOS¨CalB2 mice (Bayguinov et al., 2017). Adult mice were transcardially perfused with saline followed by 4% PFA. Brains were removed, post-fixed overnight in 4% PFA, and then equilibrated in 30% sucrose. Coronal brain sections (40 μm) were prepared using a sliding microtome. Floating sections were stored at −20 °C in 96-well plates filled with cryoprotectant solution (glycerol, ethylene glycol, and 0.1 M phosphate buffer, pH 7.4, 1:1:2 by volume), and blocked in Tris-buffered saline containing 3% normal serum and 0.25% Triton X-100. Sections were then incubated with chicken anti-GFP (1:1000, Invitrogen, A10262) primary antibody, and developed with goat anti-chicken AlexaFluor-488 (1:1000, Invitrogen, A11039) secondary antibody.

Data analysis

Initial analysis was performed with the data processing functions in Neuroplex and PhotoZ (the programs used for experiments). Fluorescence signals were divided by resting light intensity, and filtered with a binomial filter or a four-pole low-pass Butterworth filter at 500 Hz. We applied a Gaussian spatial filter to epifluorescence images and response intensity maps, and used these images together with resting light images to select regions of interest containing MC somata. The standard deviation of the pre-stimulus baseline was determined and responses were analyzed if their peak amplitude was three standard deviations from the baseline. Response latencies were taken as the time from stimulation until the response reached half of its peak amplitude. Peak amplitude, latency, and area under evoked responses were analyzed with Neuroplex or PhotoZ, and data exported to Clampfit 9.2 (Molecular Devices), and Origin 9 (OriginLab) for additional processing. Statistical tests were performed with Prism 8 (GraphPad Software) and Origin 9. One-way ANOVA with Greenhouse-Geisser correction and Dunnett’s multiple comparisons test were used when comparing multiple groups.

Results

MC targeting in hVOS::CalB2 and hVOS::Calcrl mice

hVOS probe fluorescence was abundant in the dentate gyrus of slices from both hVOS::Calcrl and hVOS::CalB2 double transgenic mice (Fig. 1). The Calcrl Cre driver has been reported to target only MCs in the dentate gyrus (Jinde et al., 2012). By contrast, in addition to targeting MCs, the CalB2 Cre driver also targets the much less abundant calretinin-expressing GABAergic interneurons (sparser in mouse than rat (C. R. Houser, 2007)) and adult-born GCs (Blasco-Ibanez & Freund, 1997; Brandt et al., 2003; Fujise, Liu, Hori, & Kosaka, 1998). The latter were unlikely to be targeted because expression was observed in the hilus rather than the subgranular zone or GCL, where calretinin-positive adult-born GCs are located (Todkar, Scotti, & Schwaller, 2012). In both hVOS::CalB2 and hVOS::Calcrl mice we observed hVOS-expressing neurons in the dentate gyrus, and the distribution of fluorescence was consistent with the anatomy of MCs (Figs. 1 and 2). Within the molecular layer, hVOS probe was confined to the inner molecular layer, consistent with the known dense innervation of proximal GC dendrites by MCs. Resting fluorescence images exhibited the characteristic horseshoe arc of the GCL, which appeared dark between the brighter hilus and inner molecular layers. This pattern of fluorescence highlighted the overall anatomy of the dentate gyrus, and aided in the analysis of spatial relations of hVOS responses from neurons in different locations.

Labeling was sparser in slices from hVOS::CalB2 mice compared to hVOS::Calcrl mice (compare Fig. 1A and 1B), but in both cases cell bodies were visible (indicated with red arrowheads in these images). To improve the evaluation of morphology, slices from transcardially perfused hVOS::CalB2 mice were fixed and labeled with anti-GFP antibodies to enhance probe fluorescence (see Methods – Morphology). In these slices (Figs. 1C and 1D) we could see the large cell bodies (indicated with red arrowheads) and dendrites with thorny excrescences (indicated with yellow arrowheads) characteristic of MCs, and consistent with their established morphology (Amaral, 1978; Scharfman, 2016). MCs exhibited strong membrane fluorescence and weak cytoplasmic fluorescence, because the hVOS probe targets the plasma membrane. The sparser labeling in slices from hVOS::CalB2 mice (Fig. 1A) is consistent with the previous report that probe expression is limited to 40% of the calbindin 2 expressing cells (Bayguinov et al., 2017). The denser labeling in hVOS::Calcrl mice reflects the high efficiency of recombination with the constitutive Calcrl Cre driver versus the conditional tamoxifen-dependent recombination with the CalB2 Cre driver. The denser labeling in slices from hVOS::Calcrl mice resulted in a high background fluorescence, which in addition to obscuring cell morphology, also reduced the signal-to-noise ratio of fluorescence changes in hVOS recordings. As a result, the hVOS signals were generally of higher quality in experiments with slices from hVOS::CalB2 mice. Nevertheless, experiments performed with each of the two crosses gave similar results.

MC responses to dentate gyrus inputs

To investigate the electrical activity of MCs, we imaged fluorescence in the hilus of hippocampal slices from mice with targeted probe expression. A resting fluorescence image from an hVOS::CalB2 slice shows the contours of the dentate gyrus (Fig. 2A – left). The

characteristic horseshoe shape of the GCL is dark with much less MC membrane than the hilus, which contains MC cell bodies and dendrites, and the inner molecular layer that contains MC axons. Stimulating in the OML predominantly activates the perforant path (PP, stimulating electrode out of view), as well as dendrites emanating from GC somata in the nearby GCL, leading to the depolarization of multiple MCs in the hilus. To view the spatial extent of these responses, we mapped the peak change in fluorescence from baseline (ΔF) within a 5–25 msec time window after stimulation and divided by resting light intensity (F). This time window excludes antidromic spikes, which with a ~100 μm/msec propagation velocity (Ma, Bayguinov, & Jackson, 2017) pass through our field of view in ~ 2 msec. Encoding ΔF/F as color revealed depolarized MCs as bright yellow-red spots on a blue background (Fig. 2A – right; the indigo-red color scale in the lower right corner indicates the magnitude of depolarization with indigo indicating no response and red indicating maximal response). The somata of 6 selected neurons are highlighted in this response intensity map with black arrowheads, but several other colored spots indicate additional neurons that responded to this stimulus. To indicate the cells we selected, Fig. 2A-left was reproduced with orange circles, numbers, and arrowheads at the 6 corresponding locations (Fig. 2A-center). Due to the lower spatial resolution (80×80) of the CCD-SMQ camera that acquired these images, they do not reveal details such as membrane labeling that are visible in the high-resolution optical sections of Fig. 1. Instead, somata of labeled cells often appear as dark holes created by the large volume of weakly fluorescent cytoplasm (Fig. 2A – left).

Fluorescence was averaged within regions that encompass MC somata and plotted versus time to reveal depolarizations as downward deflections (Fig. 2B). Depolarization moves DPA across the membrane toward the hVOS probe at the inner cell surface to quench fluorescence and decrease emission (Chanda et al., 2005). This makes hVOS probe responses nonlinear, giving them their greatest sensitivity in a roughly −100 to 0 mV window (Chanda et al., 2005; Wang et al., 2010). While this nonlinearity complicates the interpretation of amplitudes, simultaneous patch clamping and hVOS imaging in brain slices has shown that the hVOS signals faithfully track the dynamics of voltage (Bayguinov et al., 2017; Ghitani, Bayguinov, Ma, & Jackson, 2015). The fluorescence traces from the 6 highlighted MCs in Fig. 2A show that PP stimulation depolarized MCs to varying degrees. In MCs numbered 1–4, clear yellow to red spots in the response map of Fig. 2A-right correspond to distinct deflections in the fluorescence traces of Fig 2B. By contrast, the weakest responses in MCs 5 and 6 (Fig. 2B) correspond with locations in the response map with green spots.

The stimulating electrode was then moved to the GCL of this slice, where it is faintly visible in the resting fluorescence image (Fig. 2C - left). The response intensity map indicated that stimulation at this site depolarized a larger number of MCs (the 5–25 msec window excludes antidromic action potentials in MCs). The two MCs with very weak responses to PP stimulation In Figs. 2A and 2B (cells 5 and 6) gave clear responses to GCL stimulation. These neurons produced orange or red spots in the intensity map (Fig. 2C - right), and the fluorescence traces revealed robust depolarizations (Fig. 2D). Thus, in this slice GCL stimulation activated MCs more strongly than PP stimulation. Furthermore, the peak intensity map for PP responses showed very small responses in the inner molecular

layer where MC axons project (Fig. 2A - right). By contrast, the map for GCL stimulation showed strong responses of the population of MC axons in this layer (Fig. 2C - right). This experiment illustrates a general trend that GCL stimulation activated MCs more robustly than PP stimulation. This result is consistent with the idea that GCs make very strong excitatory synapses on MCs (Scharfman et al., 1990), possibly as a result of their giant boutons innervating thorny excrescences (Frotscher et al., 1991). By contrast, the PP activates MCs disynaptically through GCs. Exceptions do exist however, because MCs have some dendrites in the molecular layer that could be directly activated by our PP stimulation electrode (Azevedo et al., 2019; Scharfman, 1991).

MCs responded to PP stimulation with a long latency of 16.6 ± 2.6 msec (mean ± SD: 12 neurons, 4 slices, 4 animals). By contrast, responses to GCL stimulation had a considerably shorter latency of 4.2 ± 1.2 msec (mean ± SD, 23 neurons, 7 slices, 7 animals), with no overlap of ranges (PP range 13.4 – 22.3 msec; GCL range 1.7–8.8 msec). The longer latency with PP stimulation suggested a disynaptic response through the PP → GC → MC pathway. To test the role of GCs, we applied the mGluR 2/3 agonist DCG-IV (1 μM), which inhibits glutamate release from GC nerve terminals (Kamiya, Shinozaki, & Yamamoto, 1996). Fig. 3A presents a result with PP stimulation of an hVOS::CalB2 slice (Fig. 3A1 – left) and an hVOS::Calcrl slice (Fig. 3A2 – left). DCG-IV reduced the area and peak amplitude of responses to PP stimulation by 80% and 59%, respectively (Figs. 3B1 and 3B2, 8 neurons, 3 slices, 3 animals; for the three groups repeated measures one-way ANOVA $p = 0.0011$ and 0.0008, fir control vs. DCG-IV $p < 0.0001$ and $p = 0.0036$), and this blockade recovered when DCG-IV was removed (Fig. 3B-wash). DCG-IV was similarly effective in both hVOS::CalB2 (Figs. 3A1 and 3B1) and hVOS::Calcrl (Figs. 3A2 and 3B2) slices.

In contrast to responses evoked by PP stimulation, DCG-IV blocked response areas evoked by GCL stimulation by only 20% (Figs. 3C and 3D1). Response peak amplitude was not significantly reduced (Fig. 3 D2). This suggests that MC responses to GCL stimulation do not depend nearly as strongly on GC → MC synapses. The block ratios were significantly lower for PP stimulation than GCL stimulation (Fig. 3E1 and Fig. 3E2, $p < 0.0001$, *t*-test with Welch's correction). The very weak sensitivity of MC responses to GCL stimulation is surprising, and suggests that even though stimulation of this site activates GCs directly, other inputs to MCs are also strongly activated. Experiments presented below explore the source of these DCG-IV insensitive responses.

MC responses to CA3 back-projections

CA3 pyramidal cell axons project to the hilus and form excitatory synapses on MCs in a pathway referred to as the CA3 back-projection (Scharfman, 2007). To evaluate MC responses to the back-projection, we stimulated the CA3 region. Stimulating the CA3 stratum pyramidale (site illustrated at the top of Fig. 4A1) depolarized MCs through much of the hilus, as can be seen with response intensity maps (Fig. 4A1 - right) and fluorescence traces (Fig. 4A2). MC responses to stratum pyramidale stimulation had a mean latency of 7.9 ± 1.7 msec (mean ± SD; 11 neurons, 4 slices, 4 animals). Stimulating the neighboring stratum lucidum (site illustrated in Fig. 4C1 - top) antidromically activates the axons of dentate GCs, and this also depolarized MCs throughout much of the hilus (Figs. 4C1) with a

similar latency of 7.7 ± 1.2 msec (mean ± SD; 7 neurons, 3 slices, 2 animals). Because of the proximity of the stratum pyramidale and stratum lucidum, we sought a stimulation site for activating pyramidal cells without activating GC axons. We therefore stimulated the fimbria (site illustrated in Fig. 4E1 - top), which contains CA3 pyramidal cell axons and provides a means of activating pyramidal cells antidromically (Scharfman, 1993, 1996). Stimulating the fimbria depolarized MCs throughout much of the hilus (Figs. 4E1 and 4E2) with a latency of 15.5 ± 4.9 msec (mean ± SD; 7 neurons, 3 slices, 2 animals), which is considerably longer than the 7.9 msec latency noted above for responses to CA3 stratum pyramidale stimulation. The longer latency presumably reflects the additional time for antidromic conduction from the fimbria to CA3 pyramidal cells, and ensuing orthodromic conduction from pyramidal cells to MCs. Also, the original pyramidal cells activated antidromically by the fimbria may serve to activate area CA3c pyramidal cells, which innervate the hilus more than the pyramidal cells of CA3a–b located near the fimbria (Li, Somogyi, Ylinen, & Buzsaki, 1994).

Because of the close proximity of mossy fibers (GC axons) in the stratum lucidum to pyramidal cell bodies in the stratum pyramidale, we used DCG-IV to assess mossy fiber contributions to responses elicited by stimulation of these two sites. DCG-IV only weakly blocked MC responses to stratum pyramidale stimulation (Figs. 4B1 and 4B2), suggesting GC axons make a minor contribution to these responses. In contrast, DCG-IV blocked MC responses to stratum lucidum stimulation more strongly (Figs. 4D1 and 4D2). The weak blockade of MC responses to stratum pyramidale stimulation was not statistically significant (Fig. 4D1), but the blockade of responses to stratum lucidum stimulation was (Figs. 4B1 and 4B2; one-way ANOVA $p = 0.0072$ and 0.0003, $p = 0.005$ and 0.0002 for control versus DCG-IV). The blockades of responses to the two stimulation sites were significantly different (Figs. 4F1 and 4F2, $p = 0.0002$ for both). Thus, the responses of MCs to stratum pyramidale stimulation resulted predominately from activation of the CA3 back-projection, while the responses of MCs to stratum lucidum stimulation had a large contribution from antidromic firing of mossy fibers arising from GCs.

Although stimulating the DG activates the CA3 region, it is very unlikely that return conduction contributes to the hilar responses to GCL stimulation. Conduction to the CA3 region and back will result in latencies considerably longer than the short latencies of MC responses to GCL stimulation (Fig. 2D).

MC responses to MC stimulation

Since stimulation of the PP, GCL, and CA3 all failed to reveal the DCG-IV-insensitive excitatory inputs to MCs evoked by GCL stimulation, we considered the possibility that these responses arise from direct synaptic interactions between MCs. Thus, when GCL stimulation activates nearby MCs, those MCs could then activate other MCs further away. In support of the existence of MC → MC synapses, rabies virus tracing (Sun et al., 2017) and glutamate photorelease (Shi et al., 2019) have indicated that MCs make synaptic contacts with one another, and paired recordings have revealed rare instances of coupled pairs (Larimer & Strowbridge, 2008). To test the hypothesis of MC → MC synapses, we adopted a method for stimulating single cells that employs electrodes fabricated from theta glass with ~3 μm openings. Compared to the electrodes used for stimulation of populations, these

theta electrodes have much smaller tips, and are positioned under visual control to contact a single selected cell directly. Since the source and return current of the stimulus arise from the adjacent barrels of the theta glass, the stimulus current remains confined to the electrode tip and targets the selected cell (Cabezas and Buño, 2006). Fig. 5A displays an IR-DIC image with a theta electrode touching an MC. To verify that theta electrode stimulation only activated the selected MC, we varied the current to find the threshold. The response map using a stimulus current of 100 μA shows a weak depolarization of the stimulated cell (Fig. 5B). Increasing the stimulation current by only 20 μA depolarized the targeted MC more strongly, and this larger stimulation also depolarized a number of surrounding MCs (Fig. 5C – 120 μA). The targeted cell is indicated with a white arrow in both Fig. 5B and Fig. 5C, and black arrows in Fig. 5C indicate MCs that were not depolarized by 100 μA and were depolarized by 120 μA.

Fluorescence traces from these neurons show that 100 μA produced a weak response in the directly stimulated cell but not in the surrounding postsynaptic MCs (Fig. 5D). By contrast, 120 μA produced a rapid spike-like response in the targeted cell, indicating this stimulus was suprathreshold. Exceeding the spike threshold of the targeted cell elicited clear depolarizations in the surrounding postsynaptic MCs (Fig. 5E). Note that these responses to a single MC generally were smaller than the responses to extracellular stimulation (e.g. Figs. 2B and 2D). Extracellular stimulation activates more than one synaptic input to a given cell, while the surrounding MCs in Fig. 5E were responding to only one cell. The directly stimulated cell responded with essentially no delay, but the postsynaptic cells responded with latencies of 4.24 ± 2.67 msec (N = 10). This latency is very similar to that of responses to GCL stimulation of 4.2 msec noted above, and supports the idea that the GCL is an effective stimulation site for activating MCs. In general, with single MC stimulation the response of surrounding MCs depended on an action potential in the directly stimulated MC. The directly stimulated MCs produced rapid spikes immediately after suprathreshold stimulation while the surrounding MCs produced slower responses with the shape of a synaptic potential a few milliseconds later. These results suggest that the surrounding neurons are postsynaptic targets of the directly stimulated neuron.

To test the possible contribution of GC inputs to responses elicited by single cell MC stimulation we applied DCG-IV. Two MCs separated by ~100 μm are indicated in a resting fluorescence image in Fig. 6A1. Stimulation of the PP elicited strong responses in both cells, and the traces in Fig. 6A2 show that DCG-IV completely blocked these responses (as in Figs. 3A1, 3A2, 3B1 and 3B2). Theta electrode stimulation of neuron 1 also elicited robust responses in the two cells, with the response of neuron 2 following the response of neuron 1 by ~2 msec (Fig. 6A3). DCG-IV failed to block the response of neuron 1, as expected because this cell was stimulated directly (upper right traces in Fig. 6A3). DCG-IV also failed to block the response of neuron 2 (lower right traces in Fig. 6A3), and because release from GC terminals is blocked by DCG-IV, this experiment indicates that nerve terminals of GCs do not contribute to the synaptic response in neuron 2 elicited by stimulation of neuron 1.

We explored the role of glutamate receptors further by pharmacologically dissecting synaptic inputs using ionotropic glutamate receptor antagonists. Fig. 6B1 - left shows a resting fluorescence image highlighting two selected neurons. The AMPA receptor

antagonist NBQX (10 μM) failed to block the spike in neuron 1, as expected because this neuron was stimulated directly (top traces in Fig. 6B2). NBQX did block the later response of neuron 2 (lower traces in Fig. 6B2). In this experiment the response of neuron 1 had a second phase that peaked ~8 msec after the stimulus pulse, well after its spike. This second phase was blocked by NBQX. Thus, this second phase of the response of neuron 1 could be either an MC autapse or a disynaptic response involving other excitatory neurons (GCs or MCs). A small NBQX insensitive spike was seen in neuron 2 and this likely reflects a voltage change in neuron 1, which is only ~40 μm away and could extend processes into the region occupied by the soma of neuron 2. Similar experiments were conducted with slices from both hVOS::CalB2 and hVOS::Calcrl mice. NBQX reduced the mean response area to 37.6% of controls and peak amplitude to 53.6% of controls in slices from hVOS::CalB2 mice (Fig. 6C1; 95% confidence interval: 24.0%–51.2%); NBQX reduced the response area to 45.4% of controls and peak amplitude to 69% in slices from hVOS::Calcrl mice (Fig. 6D1; 95% confidence interval: 40.4%−75.9%). Similar results were also obtained with 1 mM kynurenic acid, a non-selective NMDA/AMPA/kainate receptor antagonist. Kynurenic acid reduced response area to 44.6% and peak amplitude to 57.7% of controls in hVOS::CalB2 (Fig. 6E1; 95% confidence interval: 23.7%−65.4%). Because kynurenic acid washes out rapidly we could demonstrate the reversal of the actions of this drug (Fig. 6E1 and Fig. 6E2 – wash). These experiments demonstrate that responses in neighboring MCs to stimulation of a single MC depend on ionotropic glutamate receptors.

Single MC Activation of the MC → GC → MC circuit

Pharmacological manipulations of glutamate receptors support the hypothesis that MC responses to MC stimulation are synaptic. Furthermore, the action of DCG-IV was often weak, supporting the hypothesis that these responses can be evoked with relatively little release from GC axons. However, blockade by DCG-IV varied, and this indicates that release from GC axons can sometimes come into play through polysynaptic activation of the MC → GC → MC circuit. Since polysynaptic responses should have a longer latency we evaluated the temporal spread of responses to stimulation of a single MC. Fig. 7A displays a sequence of peak fluorescence response maps. These maps demonstrated the onset of depolarization and its spread through the hilus. The responses in the 8–16 msec window indicate that some of the hilar MCs respond with a latency longer than expected for monosynaptic responses. As noted above, MC responses to GCL stimulation had latencies of 4.2 ± 1.2 msec, and these responses are presumably monosynaptic. Although there synaptic delays are intrinsically variable, a response latency that is roughly twice as long, > ~ 8 msec, is very likely to be mediated by more than one synapse. Since responses mediated by the MC → GC → MC circuit should have a longer latency, DCG-IV should block later responses more effectively than early responses. The sequence of response maps in the lower row of Fig. 7A show more effective block in the later time windows than the early time window, suggesting greater block of long latency, presumably polysynaptic responses.

The relation between latency and DCG-IV sensitivity was examined further by analyzing fluorescence traces from MCs. Fig. 7B shows a response in a stimulated neuron (neuron 1) and a short-latency response in its postsynaptic target (neuron 2). Fig. 7C shows a similar example but the response in the second cell had a longer latency. In both examples, DCG-IV

did not block the response in neuron 1 to direct theta electrode stimulation. Turning to the second cell with a longer latency (Fig. 7C), DCG-IV did not block the short latency direct response but did block the longer latency response in the second cell. To evaluate the effect of DCG-IV on responses with different latencies, responses were separated into three time windows and the response (area above baseline and peak amplitude) within each window was evaluated. For responses in the 0–8 msec time window, DCG-IV had no significant effect, indicating that GC axons do not contribute to fast responses (Figs. 7D1 and 7D2). In the 8–16 msec time window DCG-IV blocked by almost 50%, and the block was highly significant. A small but significant block by DCG-IV was also seen in the 16–24 msec window. The weaker block in this later window may reflect the slower decay of MC → MC EPSPs of ~10 msec (Larimer & Strowbridge, 2008) compared to the rapid decay of GC→MC EPSPs of ~5 msec (Scharfman, 1995). These results indicate that GC axons make little contribution to short latency responses of MCs evoked by MC stimulation, but do contribute to longer latency responses. The association of longer latency with greater DCG-IV sensitivity supports the hypothesis that a single MC can activate other MCs both directly and through the MC → GC → MC circuit.

MC Connectivity

The response intensity maps for single MC stimulation in Figs. 6 and 7 and the differential blockade of short and long latency responses (Figs. 7D1 and 7D2) suggest that MC activity spreads to other MCs by two routes, monosynaptically through MC → MC synapses and polysynaptically through the MC → GC → MC circuit. In 43 slices with single MC stimulation, we observed 404 MCs with responses more than 3 standard deviations above baseline. In the 0–8 msec window, which corresponds primarily to monosynaptic MC → MC responses, the average number of responsive MCs in a slice was 2.7 (median 1, range 0–30). In the 8–16 msec time window, which corresponds to polysynaptic MC → GC → MC responses, the average number of responsive MCs in a slice was 5.3 (median 3.5, range 0–34). We measured the distances to responsive MCs and found that MCs activated in the monosynaptic time window were 95.5 ± 55.5 μm (mean ± SD, range 27 – 252 μm, N = 74) from the stimulated MC. MCs activated in the disynaptic window overlapped in distance but on average were significantly farther away from the stimulated MC (mean 110.3 ± 61.0 μm, N = 226, range 27 – 320 μm, p = 0.031, Mann-Whitney test).

The numbers of synaptically coupled MCs are likely to be underestimates because of the reduced connectivity in brain slices where an unknown number of axons have been severed during slice preparation. Furthermore, our criterion of 3 standard deviations above baseline left weakly responsive cells uncounted. Thus, the numbers of responsive cells reported here can be viewed as a lower bound to the number of locally coupled MCs in the hilus. This estimate does not include connectivity between MCs along the longitudinal axis of the hippocampus. These results nevertheless indicate that both monosynaptic and polysynaptic communication between MCs are common and are likely to contribute significantly to dentate gyrus functions.

Discussion

The present study targeted an hVOS sensor to hilar MCs in order to image their voltage changes in response to various inputs. Stimulation of the PP, GCL, and CA3 region all depolarized MCs in a manner consistent with their known synaptic inputs. However, the failure of DCG-IV to block responses to GCL stimulation raised the possibility that GCL stimulation activates a significant number of MCs directly. MCs are distributed throughout the hilus and some are close to the GCL. MCs also have processes extending into the GCL. When GCL stimulation activates MCs, they in turn can activate other MCs through direct synaptic contacts. In support of this idea, stimulation of single MCs revealed synaptic responses in other MCs with short latencies. The pharmacological sensitivities of these responses were consistent with direct synaptic coupling between pairs of MCs. This work thus confirms and extends prior reports of synaptic coupling between MCs (Larimer & Strowbridge, 2008; Shi et al., 2019; Sun et al., 2017). The labeling and imaging strategies employed here may aid in guiding efforts to make electrophysiological recordings from MCs, both individually and pairwise. Such experiments would enhance studies MC→MC connectivity and enable the quantitative characterization these synapses. In addition, MC responses to single MC stimulation included responses with longer latency, and with a pharmacological sensitivity reflecting the involvement of a polysynaptic circuit formed by mutually excitatory MCs and GCs. These results illustrate the power of using Cre-lox based targeting together with an hVOS Cre reporter to investigate the physiology and circuitry of genetically-defined neurons (Bayguinov et al., 2017). Using two different targeting methods, hVOS⁞Calcrl and hVOS⁞CalB2, imaging with this hybrid genetically-encoded voltage sensor revealed that hilar MCs integrate diverse inputs from various types of hippocampal neurons including other MCs.

Targeting MCs

MCs are distributed throughout the hilus where they are surrounded by other types of neurons and neuropil. They are thus more difficult to find and manipulate than many other types of neurons. These challenges have motivated efforts to develop methods for targeting MCs. One approach is to exploit the commissural projections by injecting retrograde dye (Ratzliff, Howard, Santhakumar, Osapay, & Soltesz, 2004) or viral expression vectors (T. T. Hsu, Lee, Tai, & Lien, 2016) into the hilus. Another approach is to use mouse lines with Cre recombinase in MCs and inject viral constructs encoding opsins or DREADDs (Botterill et al., 2019; Botterill et al., 2021) or cross the Cre lines with reporter mice (C.R. Houser et al., 2021). In the present study we used two Cre-driver lines to target hVOS probe to MCs. The CalB2 gene (encoding the protein calretinin) targets MCs in the ventral dentate gyrus, adult-born granule cells, and some GABAergic interneurons (Blasco-Ibanez & Freund, 1997; Brandt et al., 2003; Fujise et al., 1998; C. R. Houser, 2007). There are fewer calretinin-positive GABAergic cells in mouse compared to rat (C. R. Houser, 2007), and they are located mostly at the interface between the hilus and GCL. Adult-born GCs are sparse and can usually be distinguished by location and morphology. Thus, even though CalB2 targets some other cell types, they are quite sparse and in distinct locations relative to MCs. Therefore, hVOS probe-expressing neurons in the hilus are predominantly MCs. The Calcrl-Cre driver line drives expression in the CA3 region and cortex as well as the

hilus (Bayguinov et al., 2017; C.R. Houser et al., 2021; Jinde et al., 2012), but in the hilus this Cre driver only labels MCs. Calcrl-Cre mice produced better targeting specificity in the hilus, while CalB2 Cre produced sparser labeling, lower background, and better signal-to-noise. These two Cre drivers both provided readouts from MCs of their electrical responses to stimulation of the PP, GCL, and CA3 region, and thus validated the well-established synaptic inputs to MCs. The two targeting vehicles used here have complementary strengths and weaknesses, and the similar results obtained with both provide assurance that we were interrogating MCs. The similar results with two different targeting methods also supports our conclusions.

Activation of MCs

PP, GCL, and CA3 stimulation all activated MCs, and the longer latency of responses to PP stimulation indicates a sequence of PP activation of GCs, leading to GC mossy fiber activation of MCs. GCL stimulation activated MCs more strongly than PP stimulation and with shorter latency. The dependence of responses to PP stimulation on mossy fibers was demonstrated by the strong blockade of these responses by DCG-IV. However, it comes as a surprise that the robust responses of MCs to GCL stimulation were insensitive to DCG-IV. The relative extent to which GCL stimulation activates MC versus GC inputs to MCs may vary with on slice orientation, and our use of horizontal slices may favor the DCG-IV insensitive contribution. Our results support the hypothesis that GCL stimulation activates MCs directly. Depolarization of directly activated MCs spreads to other MCs by glutamatergic synapses (Fig. 6). Our response maps and resting fluorescence images indicate that slices have many MCs at the GCL border, and GCL stimulation can activate these MCs. Furthermore, MC axons pass through the GCL to project to the inner molecular layer and some MC dendrites extend to the molecular layer (Scharfman, 2016). Thus, the MC→MC synapses provide a route through which GCL stimulation can activate MCs robustly, and independently of GCs.

Functional implication of MC → MC synapses

According to the work of Sun et al. (2017), hilar neurons account for 22.9% of the synaptic inputs to MCs and 2/3 of these are GABA negative. MCs also receive a sparse direct input from entorhinal cortex, which accounts for only 0.1% of their synaptic inputs, and an input from CA3 pyramidal cells that accounts for 6.35% of their synaptic inputs. Other studies suggest the PP input may be greater (Azevedo et al., 2019; Scharfman, 1991) but the available information does suggest that MCs receive a substantial input from other hilar neurons. The present work showed that stimulating the GCL elicited short-latency depolarizations in MCs that could not be blocked by DCG-IV, suggesting that these responses do not depend on release from GC axons (Fig. 3). Stimulating single MCs individually with small-tipped theta glass electrodes elicited responses in neighboring MCs. The response of the directly stimulated neuron was graded with stimulus strength, and could be gauged as sub- or suprathreshold by the magnitude and shape of the fluorescence change. The stimulated cell exhibited a threshold as the stimulus current increased, and neighboring cells responded only when the directly stimulated cell fired an action potential. The responses of these neighboring cells depended on glutamate receptors, and those with short latency were insensitive to DCG-IV. These experiments thus support the existence

of functional synapses between MCs. This confirms previous rabies virus tracing studies that suggested anatomical connections (Sun et al., 2017), as well as a report that uncaging glutamate in the hilus activates synapses on MCs (Shi et al., 2019). The lower incidence of coupling seen with paired intracellular recording (Larimer & Strowbridge, 2008) may reflect the younger age of the animals (p14–21) or species (rats) or greater difficulty of sampling pairs with this technically difficult approach. Our data suggest that MC-MC synapses are a significant element of hilar circuitry. It will be interesting in the future to determine whether MC → MC synapses are sensitive to CB1 receptor agonists like their terminals in the inner molecular layer (Castillo, Younts, Chavez, & Hashimotodani, 2012), and whether MC-MC synapses exhibit LTP like other MC synapses in the DG (Hashimotodani et al., 2017; Lysetskiy, Foldy, & Soltesz, 2005; Wright & Jackson, 2014).

c-fos expression indicates that MCs are active *in vivo* (Duffy, Schaner, Chin, & Scharfman, 2013) and that this activity plays a role in the detection of novelty (Bernstein, Lu, Botterill, & Scharfman, 2019). Previous *in vivo* recording in the dentate gyrus showed that MCs are more likely to have multiple place fields in a single context, compared to GCs and CA3 pyramidal cells, which have single place fields (Danielson et al., 2017; GoodSmith et al., 2017). Recordings from putative monosynaptic GC-MC pairs showed that a MC discharged at a place where the presynaptic GC was silent, suggesting converging inputs to MCs (Senzai & Buzsaki, 2017). Given that GCs fire sparsely and exhibit single place fields, synapses between MCs could play an important role in extending the MC place fields beyond those of their presynaptic GC inputs. Thus, it is possible that MC → MC synapses integrate and process upstream place field information from GCs.

Mounting evidence from slice and *in vivo* recording supports the idea that MCs should be considered as a second principal cell type in the dentate gyrus rather than an excitatory interneuron. The GC → MC → GC circuit has long been recognized for its potential in redistributing activity between different sets of GCs (Buckmaster & Schwartzkroin, 1994; Henze & Buzsaki, 2007; Scharfman, 2016). The finding of long latency DCG-IV sensitive responses of MCs to action potentials in a single MC adds a variation to this idea. This suggests that the GC → MC → GC circuit can be set into motion by just one MC. MC → MC synapses would amplify regenerative excitation in the hilus and may contribute to the prolonged bursts of synaptic potentials that follow the depolarization of a single MC (Strowbridge & Schwartzkroin, 1996). Thus, the activation of MCs may serve as a critical event in the gating of the dentate gyrus (D. Hsu, 2007).

MC → MC synapses add a new dimension to the processing capabilities of the dentate gyrus. Like the mutual excitation between GCs and MCs, direct excitation between MCs can also serve to redistribute inputs within the dentate gyrus, thus reinforcing, extending, and complementing the GC → MC → GC circuit. Exploring how MCs compute their heterogeneous inputs, and how synaptic plasticity alters these computations, will shed light on hippocampal functions such as spatial navigation and pattern separation. MC → MC synapses also offer a new locus of mutual excitation that can influence the excitation/inhibition balance of the dentate gyrus, alter its gating functions (D. Hsu, 2007), and influence the generation and spread of epileptic seizures (Botterill et al., 2019; Bui et al., 2018; Dudek & Sutula, 2007; Ratzliff et al., 2002; Scharfman, 2016; Sloviter, 1994).

Funding information

National Institute of Neurological Disorders and Stroke grants NS093866, MH109305, NS098767, and NS105200

The data that support the findings of this study are available from the corresponding author upon reasonable request.

References

Amaral DG (1978). A Golgi study of cell types in the hilar region of the hippocampus in the rat. J Comp Neurol, 182(4 Pt 2), 851–914. doi:10.1002/cne.901820508 [PubMed: 730852]

Amaral DG, Scharfman HE, & Lavenex P (2007). The dentate gyrus: fundamental neuroanatomical organization (dentate gyrus for dummies). Prog Brain Res, 163, 3–22. doi:S0079–6123(07)63001–5 [pii]10.1016/S0079-6123(07)63001-5 [PubMed: 17765709]

Azevedo EP, Pomeranz L, Cheng J, Schneeberger M, Vaughan R, Stern SA, … Friedman JM (2019). A Role of Drd2 Hippocampal Neurons in Context-Dependent Food Intake. Neuron, 102(4), 873–886 e875. doi:10.1016/j.neuron.2019.03.011 [PubMed: 30930044]

Bayguinov PO, Ghitani N, Jackson MB, & Basso MA (2015). A hard-wired priority map in the superior colliculus shaped by asymmetric inhibitory circuitry. J Neurophysiol, 114(1), 662–676. doi:10.1152/jn.00144.2015 [PubMed: 25995346]

Bayguinov PO, Ma Y, Gao Y, Zhao X, & Jackson MB (2017). Imaging Voltage in Genetically Defined Neuronal Subpopulations with a Cre Recombinase-Targeted Hybrid Voltage Sensor. J Neurosci, 37(38), 9305–9319. doi:10.1523/JNEUROSCI.1363-17.2017 [PubMed: 28842412]

Bernstein HL, Lu YL, Botterill JJ, & Scharfman HE (2019). Novelty and Novel Objects Increase c-Fos Immunoreactivity in Mossy Cells in the Mouse Dentate Gyrus. Neural Plast, 2019, 1815371. doi:10.1155/2019/1815371 [PubMed: 31534449]

Blackstad JS, Osen KK, Scharfman HE, Storm-Mathisen J, Blackstad TW, & Leergaard TB (2016). Observations on hippocampal mossy cells in mink (Neovison vison) with special reference to dendrites ascending to the granular and molecular layers. Hippocampus, 26(2), 229–245. doi:10.1002/hipo.22518 [PubMed: 26286893]

Blasco-Ibanez JM, & Freund TF (1997). Distribution, ultrastructure, and connectivity of calretinin-immunoreactive mossy cells of the mouse dentate gyrus. Hippocampus, 7(3), 307–320. doi:10.1002/(SICI)1098-1063(1997)7:3<307::AID-HIPO6>3.0.CO;2-H [PubMed: 9228528]

Botterill JJ, Lu YL, LaFrancois JJ, Bernstein HL, Alcantara-Gonzalez D, Jain S, … Scharfman HE (2019). An Excitatory and Epileptogenic Effect of Dentate Gyrus Mossy Cells in a Mouse Model of Epilepsy. Cell Rep, 29(9), 2875–2889 e2876. doi:10.1016/j.celrep.2019.10.100 [PubMed: 31775052]

Botterill JJ, Vinod KY, Gerencer KJ, Teixeira CM, LaFrancois JJ, & Scharfman HE (2021). Bidirectional regulation of cognitive and anxiety-like behaviors by dentate gyrus mossy cells in male and female mice. Journal of Neuroscience, JN-RM-1724–1720. doi:10.1523/jneurosci.1724-20.2021

Brandt MD, Jessberger S, Steiner B, Kronenberg G, Reuter K, Bick-Sander A, … Kempermann G (2003). Transient calretinin expression defines early postmitotic step of neuronal differentiation in adult hippocampal neurogenesis of mice. Mol Cell Neurosci, 24(3), 603–613. doi:S1044743103002070 [pii] [PubMed: 14664811]

Buckmaster PS, & Schwartzkroin PA (1994). Hippocampal mossy cell function: a speculative view. Hippocampus, 4(4), 393–402. doi:10.1002/hipo.450040402 [PubMed: 7874231]

Buckmaster PS, Strowbridge BW, Kunkel DD, Schmiege DL, & Schwartzkroin PA (1992). Mossy cell axonal projections to the dentate gyrus molecular layer in the rat hippocampal slice. Hippocampus, 2(4), 349–362. doi:10.1002/hipo.450020403 [PubMed: 1284975]

Buckmaster PS, Wenzel HJ, Kunkel DD, & Schwartzkroin PA (1996). Axon arbors and synaptic connections of hippocampal mossy cells in the rat in vivo. J Comp Neurol, 366(2), 271–292. [PubMed: 8698887]

Bui AD, Nguyen TM, Limouse C, Kim HK, Szabo GG, Felong S, … Soltesz I (2018). Dentate gyrus mossy cells control spontaneous convulsive seizures and spatial memory. Science, 359(6377), 787–790. doi:10.1126/science.aan4074 [PubMed: 29449490]

Cabezas C, & Buno W (2006). Distinct transmitter release properties determine differences in short-term plasticity at functional and silent synapses. J Neurophysiol, 95(5), 3024–3034. doi:00739.2005 [pii]10.1152/jn.00739.2005 [PubMed: 16436482]

Castillo PE, Younts TJ, Chavez AE, & Hashimotodani Y (2012). Endocannabinoid signaling and synaptic function. Neuron, 76(1), 70–81. doi:10.1016/j.neuron.2012.09.020 [PubMed: 23040807]

Chancey JH, Poulsen DJ, Wadiche JI, & Overstreet-Wadiche L (2014). Hilar mossy cells provide the first glutamatergic synapses to adult-born dentate granule cells. J Neurosci, 34(6), 2349–2354. doi:10.1523/JNEUROSCI.3620-13.2014 [PubMed: 24501373]

Chanda B, Blunck R, Faria LC, Schweizer FE, Mody I, & Bezanilla F (2005). A hybrid approach to measuring electrical activity in genetically specified neurons. Nat Neurosci, 8(11), 1619–1626. doi:nn1558 [pii]10.1038/nn1558 [PubMed: 16205716]

Chang PY-P (2006). Heterogeneous spatial patterns of long-term potentiation in hippocampal slices. (Ph. D.), University of Wisconsin, Madison.

Danielson NB, Turi GF, Ladow M, Chavlis S, Petrantonakis PC, Poirazi P, & Losonczy A (2017). In Vivo Imaging of Dentate Gyrus Mossy Cells in Behaving Mice. Neuron, 93(3), 552–559 e554. doi:10.1016/j.neuron.2016.12.019 [PubMed: 28132825]

Dudek FE, & Sutula TP (2007). Epileptogenesis in the dentate gyrus: a critical perspective. Prog Brain Res, 163, 755–773. doi:S0079–6123(07)63041–6 [pii]10.1016/S0079-6123(07)63041-6 [PubMed: 17765749]

Duffy AM, Schaner MJ, Chin J, & Scharfman HE (2013). Expression of c-fos in hilar mossy cells of the dentate gyrus in vivo. Hippocampus, 23(8), 649–655. doi:10.1002/hipo.22138 [PubMed: 23640815]

Frotscher M, Seress L, Schwerdtfeger WK, & Buhl E (1991). The mossy cells of the fascia dentata: a comparative study of their fine structure and synaptic connections in rodents and primates. J Comp Neurol, 312(1), 145–163. doi:10.1002/cne.903120111 [PubMed: 1744242]

Fujise N, Liu Y, Hori N, & Kosaka T (1998). Distribution of calretinin immunoreactivity in the mouse dentate gyrus: II. Mossy cells, with special reference to their dorsoventral difference in calretinin immunoreactivity. Neuroscience, 82(1), 181–200. doi:S0306452297002613 [pii] [PubMed: 9483514]

Gangarossa G, Longueville S, De Bundel D, Perroy J, Herve D, Girault JA, & Valjent E (2012). Characterization of dopamine D1 and D2 receptor-expressing neurons in the mouse hippocampus. Hippocampus, 22(12), 2199–2207. doi:10.1002/hipo.22044 [PubMed: 22777829]

Ghitani N, Bayguinov PO, Ma Y, & Jackson MB (2015). Single-trial imaging of spikes and synaptic potentials in single neurons in brain slices with genetically encoded hybrid voltage sensor. J Neurophysiol, 113(4), 1249–1259. doi:10.1152/jn.00691.2014 [PubMed: 25411462]

GoodSmith D, Chen X, Wang C, Kim SH, Song H, Burgalossi A, … Knierim JJ (2017). Spatial Representations of Granule Cells and Mossy Cells of the Dentate Gyrus. Neuron, 93(3), 677–690 e675. doi:10.1016/j.neuron.2016.12.026 [PubMed: 28132828]

Hashimotodani Y, Nasrallah K, Jensen KR, Chavez AE, Carrera D, & Castillo PE (2017). LTP at Hilar Mossy Cell-Dentate Granule Cell Synapses Modulates Dentate Gyrus Output by Increasing Excitation/Inhibition Balance. Neuron, 95(4), 928–943 e923. doi:10.1016/j.neuron.2017.07.028 [PubMed: 28817805]

Henze DA, & Buzsaki G (2007). Hilar mossy cells: functional identification and activity in vivo. Prog Brain Res, 163, 199–216. doi:S0079–6123(07)63012-X [pii]10.1016/S0079-6123(07)63012-X [PubMed: 17765720]

Houser CR (2007). Interneurons of the dentate gyrus: an overview of cell types, terminal fields and neurochemical identity. Prog Brain Res, 163, 217–232. doi:10.1016/S0079-6123(07)63013-1 [PubMed: 17765721]

Houser CR, Peng Z, Wei X, Huang CS, & Mody I (2021). Mossy Cells in the Dorsal and Ventral Dentate Gyrus Differ in Their Patterns of Axonal Projections. The Journal of Neuroscience, 41(5), 991–1004. doi:10.1523/jneurosci.2455-20.2020 [PubMed: 33268544]

Hsu D (2007). The dentate gyrus as a filter or gate: a look back and a look ahead. Prog Brain Res, 163, 601–613. doi:S0079–6123(07)63032–5 [pii]10.1016/S0079-6123(07)63032-5 [PubMed: 17765740]

Hsu TT, Lee CT, Tai MH, & Lien CC (2016). Differential Recruitment of Dentate Gyrus Interneuron Types by Commissural Versus Perforant Pathways. Cereb Cortex, 26(6), 2715–2727. doi:10.1093/cercor/bhv127 [PubMed: 26045570]

Jackson MB, & Scharfman HE (1996). Positive feedback from hilar mossy cells to granule cells in the dentate gyrus revealed by voltage-sensitive dye and microelectrode recording. J Neurophysiol, 76(1), 601–616. doi:10.1152/jn.1996.76.1.601 [PubMed: 8836247]

Jinde S, Zsiros V, Jiang Z, Nakao K, Pickel J, Kohno K, … Nakazawa K (2012). Hilar mossy cell degeneration causes transient dentate granule cell hyperexcitability and impaired pattern separation. Neuron, 76(6), 1189–1200. doi:S0896–6273(12)00957–9 [pii] 10.1016/j.neuron.2012.10.036 [PubMed: 23259953]

Jinde S, Zsiros V, & Nakazawa K (2013). Hilar mossy cell circuitry controlling dentate granule cell excitability. Front Neural Circuits, 7, 14. doi:10.3389/fncir.2013.00014 [PubMed: 23407806]

Kamiya H, Shinozaki H, & Yamamoto C (1996). Activation of metabotropic glutamate receptor type 2/3 suppresses transmission at rat hippocampal mossy fibre synapses. J Physiol, 493 (Pt 2), 447–455. [PubMed: 8782108]

Lagace DC, Whitman MC, Noonan MA, Ables JL, DeCarolis NA, Arguello AA, … Eisch AJ (2007). Dynamic contribution of nestin-expressing stem cells to adult neurogenesis. J Neurosci, 27(46), 12623–12629. doi:10.1523/JNEUROSCI.3812-07.2007 [PubMed: 18003841]

Larimer P, & Strowbridge BW (2008). Nonrandom local circuits in the dentate gyrus. J Neurosci, 28(47), 12212–12223. doi:28/47/12212 [pii]10.1523/JNEUROSCI.3612-08.2008 [PubMed: 19020015]

Larimer P, & Strowbridge BW (2010). Representing information in cell assemblies: persistent activity mediated by semilunar granule cells. Nat Neurosci, 13(2), 213–222. doi:nn.2458 [pii] 10.1038/nn.2458 [PubMed: 20037579]

Li XG, Somogyi P, Ylinen A, & Buzsaki G (1994). The hippocampal CA3 network: an in vivo intracellular labeling study. J Comp Neurol, 339(2), 181–208. doi:10.1002/cne.903390204 [PubMed: 8300905]

Lisman JE (1999). Relating hippocampal circuitry to function: recall of memory sequences by reciprocal dentate-CA3 interactions. Neuron, 22(2), 233–242. doi:10.1016/s0896-6273(00)81085-5 [PubMed: 10069330]

Lysetskiy M, Foldy C, & Soltesz I (2005). Long- and short-term plasticity at mossy fiber synapses on mossy cells in the rat dentate gyrus. Hippocampus, 15(6), 691–696. doi:10.1002/hipo.20096 [PubMed: 15986406]

Ma Y, Bayguinov PO, & Jackson MB (2017). Action Potential Dynamics in Fine Axons Probed with an Axonally Targeted Optical Voltage Sensor. eNeuro, 4(4). doi:10.1523/ENEURO.0146-17.2017

Morgan RJ, Santhakumar V, & Soltesz I (2007). Modeling the dentate gyrus. Prog Brain Res, 163, 639–658. doi:S0079–6123(07)63035–0 [pii]10.1016/S0079-6123(07)63035-0 [PubMed: 17765743]

Myers CE, & Scharfman HE (2009). A role for hilar cells in pattern separation in the dentate gyrus: a computational approach. Hippocampus, 19(4), 321–337. doi:10.1002/hipo.20516 [PubMed: 18958849]

Myers CE, & Scharfman HE (2011). Pattern separation in the dentate gyrus: a role for the CA3 backprojection. Hippocampus, 21(11), 1190–1215. doi:10.1002/hipo.20828 [PubMed: 20683841]

Ratzliff AH, Howard AL, Santhakumar V, Osapay I, & Soltesz I (2004). Rapid deletion of mossy cells does not result in a hyperexcitable dentate gyrus: implications for epileptogenesis. J Neurosci, 24(9), 2259–2269. doi:10.1523/JNEUROSCI.5191-03.200424/9/2259 [pii] [PubMed: 14999076]

Ratzliff AH, Santhakumar V, Howard A, & Soltesz I (2002). Mossy cells in epilepsy: rigor mortis or vigor mortis? Trends Neurosci, 25(3), 140–144. doi:10.1016/s0166-2236(00)02122-6 [PubMed: 11852145]

Ribak CE, Seress L, & Amaral DG (1985). The development, ultrastructure and synaptic connections of the mossy cells of the dentate gyrus. J Neurocytol, 14(5), 835–857. [PubMed: 2419523]

Santhakumar V, Bender R, Frotscher M, Ross ST, Hollrigel GS, Toth Z, & Soltesz I (2000). Granule cell hyperexcitability in the early post-traumatic rat dentate gyrus: the 'irritable mossy cell' hypothesis. J Physiol, 524 Pt 1, 117–134. doi:10.1111/j.1469-7793.2000.00117.x [PubMed: 10747187]

Scharfman HE (1991). Dentate hilar cells with dendrites in the molecular layer have lower thresholds for synaptic activation by perforant path than granule cells. J Neurosci, 11(6), 1660–1673. [PubMed: 2045880]

Scharfman HE (1993). Activation of dentate hilar neurons by stimulation of the fimbria in rat hippocampal slices. Neurosci Lett, 156(1–2), 61–66. doi:10.1016/0304-3940(93)90440-v [PubMed: 8105429]

Scharfman HE (1995). Electrophysiological evidence that dentate hilar mossy cells are excitatory and innervate both granule cells and interneurons. J Neurophysiol, 74(1), 179–194. [PubMed: 7472322]

Scharfman HE (1996). Conditions required for polysynaptic excitation of dentate granule cells by area CA3 pyramidal cells in rat hippocampal slices. Neuroscience, 72(3), 655–668. doi:10.1016/0306-4522(95)00569-2 [PubMed: 9157312]

Scharfman HE (2007). The CA3 "backprojection" to the dentate gyrus. Prog Brain Res, 163, 627–637. doi:10.1016/S0079-6123(07)63034-9 [PubMed: 17765742]

Scharfman HE (2016). The enigmatic mossy cell of the dentate gyrus. Nat Rev Neurosci, 17(9), 562–575. doi:10.1038/nrn.2016.87 [PubMed: 27466143]

Scharfman HE (2018). Advances in understanding hilar mossy cells of the dentate gyrus. Cell Tissue Res, 373(3), 643–652. doi:10.1007/s00441-017-2750-5 [PubMed: 29222692]

Scharfman HE, Kunkel DD, & Schwartzkroin PA (1990). Synaptic connections of dentate granule cells and hilar neurons: results of paired intracellular recordings and intracellular horseradish peroxidase injections. Neuroscience, 37(3), 693–707. doi:0306–4522(90)90100-I [pii] [PubMed: 2247219]

Scharfman HE, & Schwartzkroin PA (1988). Electrophysiology of morphologically identified mossy cells of the dentate hilus recorded in guinea pig hippocampal slices. J Neurosci, 8(10), 3812–3821. [PubMed: 2461436]

Senzai Y, & Buzsaki G (2017). Physiological Properties and Behavioral Correlates of Hippocampal Granule Cells and Mossy Cells. Neuron, 93(3), 691–704 e695. doi:10.1016/j.neuron.2016.12.011 [PubMed: 28132824]

Shi Y, Grieco SF, Holmes TC, & Xu X (2019). Development of Local Circuit Connections to Hilar Mossy Cells in the Mouse Dentate Gyrus. eNeuro, 6(2). doi:10.1523/ENEURO.0370-18.2019

Sloviter RS (1994). The functional organization of the hippocampal dentate gyrus and its relevance to the pathogenesis of temporal lobe epilepsy. Ann Neurol, 35(6), 640–654. doi:10.1002/ana.410350604 [PubMed: 8210220]

Strowbridge BW, & Schwartzkroin PA (1996). Transient potentiation of spontaneous EPSPs in rat mossy cells induced by depolarization of a single neurone. J Physiol, 494 (Pt 2), 493–510. doi:10.1113/jphysiol.1996.sp021508 [PubMed: 8842007]

Sun Y, Grieco SF, Holmes TC, & Xu X (2017). Local and Long-Range Circuit Connections to Hilar Mossy Cells in the Dentate Gyrus. eNeuro, 4(2). doi:10.1523/ENEURO.0097-17.2017

Todkar K, Scotti AL, & Schwaller B (2012). Absence of the calcium-binding protein calretinin, not of calbindin D-28k, causes a permanent impairment of murine adult hippocampal neurogenesis. Front Mol Neurosci, 5, 56. doi:10.3389/fnmol.2012.00056 [PubMed: 22536174]

Wang D, Zhang Z, Chanda B, & Jackson MB (2010). Improved probes for hybrid voltage sensor imaging. Biophys J, 99(7), 2355–2365. doi:10.1016/j.bpj.2010.07.037 [PubMed: 20923671]

Williams PA, Larimer P, Gao Y, & Strowbridge BW (2007). Semilunar granule cells: glutamatergic neurons in the rat dentate gyrus with axon collaterals in the inner molecular layer. J Neurosci, 27(50), 13756–13761. doi:10.1523/JNEUROSCI.4053-07.2007 [PubMed: 18077687]

Wright BJ, & Jackson MB (2014). Long-term potentiation in hilar circuitry modulates gating by the dentate gyrus. J Neurosci, 34(29), 9743–9753. doi:10.1523/JNEUROSCI.0814-14.2014 [PubMed: 25031412]

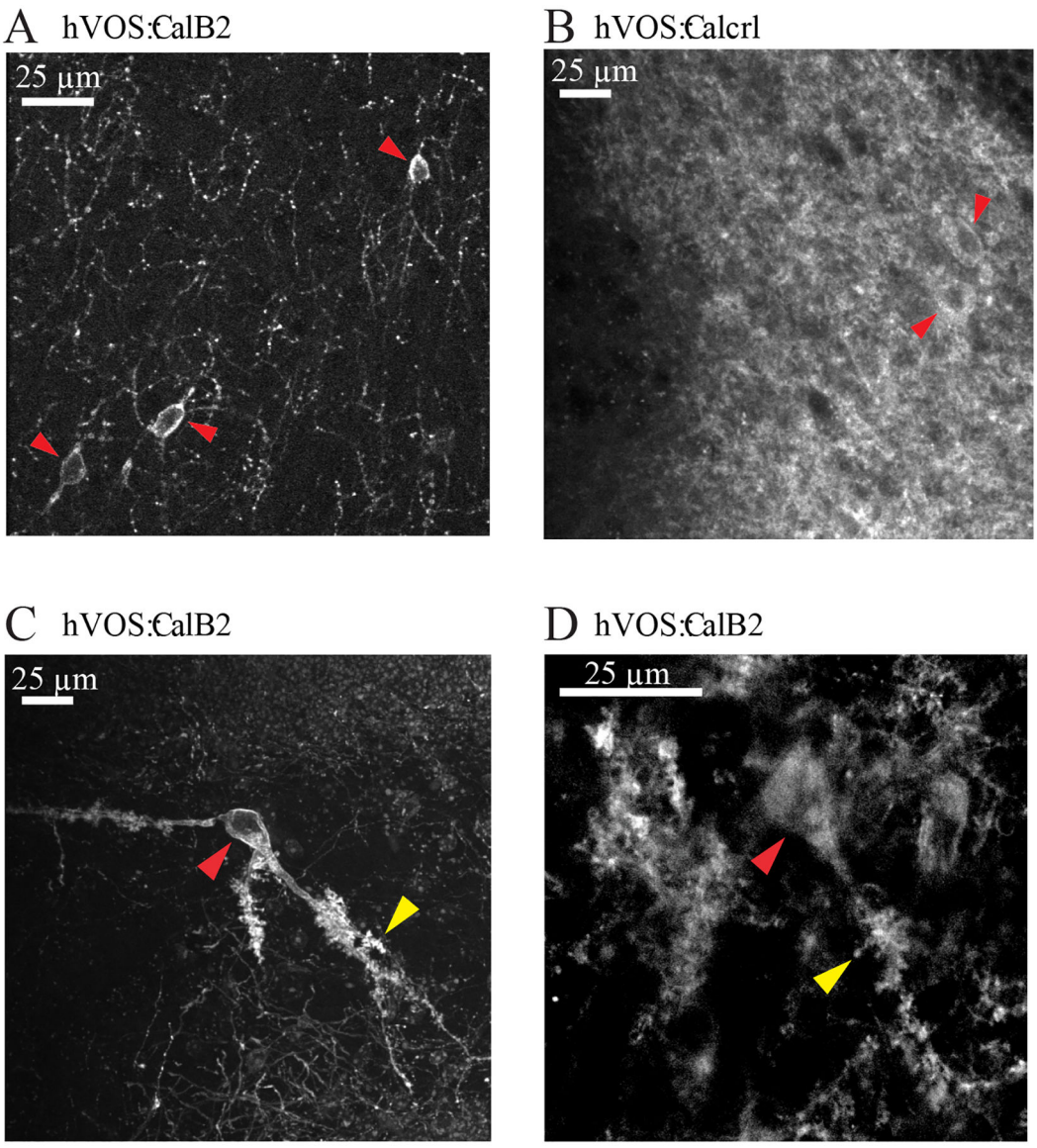

Figure 1.

hVOS probe expression in hilar MCs from hVOS::CalB2 and hVOS::Calcrl mice, imaged with two-photon microscopy. **A.** Unenhanced hVOS probe fluorescence in the hilus of a tamoxifen-injected hVOS::CalB2 animal. The sparse labeling achieved with this Cre driver leads to clearer fluorescence in targeted MCs (red arrowheads). **B.** Unenhanced hVOS probe fluorescence in the hilus of an hVOS::Calcrl animal. The high efficiency labeling with this Cre driver produced higher background; cell bodies are marked with red arrowheads. **C.** hVOS probe fluorescence enhanced by labeling with antibody against GFP (cell bodies marked with red arrowheads; large thorny excrescences arked with yellow arrowheads). **D.** Image as in **C** but at a higher magnification to highlight thorny excrescences.

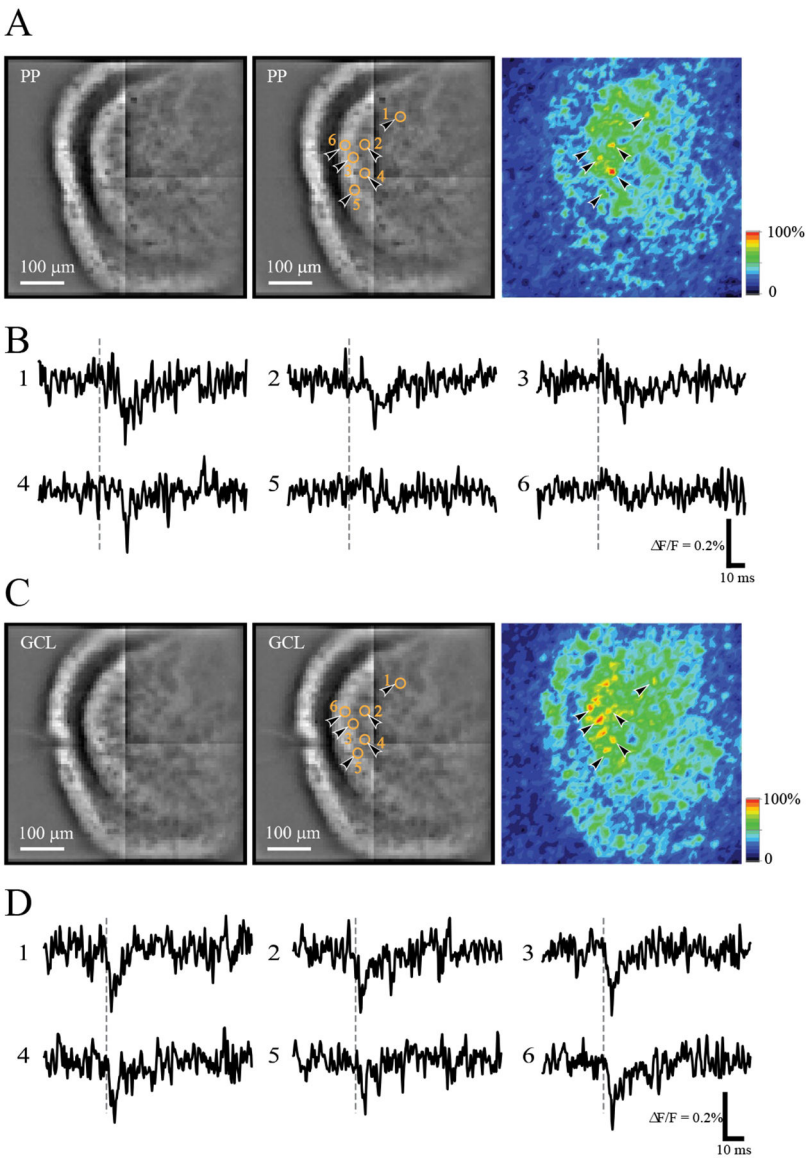

Figure 2.

hVOS imaging of MC responses to stimulation of the perforant path (PP) and granule cell layer (GCL). **A.** MC responses in an hVOS::CalB2 slice evoked by stimulation of the PP (75 μA; the stimulation electrode is just outside the field of view to the left). Left - resting fluorescence taken with the CCD-SMQ camera. Bright labeling in the hilus and inner molecular layer arises from MC somata and processes. Center - the same image with the locations of selected responsive MCs indicated by black arrowheads and orange circles; numbers correspond to the traces displayed in **B**. Right - the same field of view, mapping the peak fluorescence change in the 5–25 msec post-stimulus time window. This response intensity map displays stimulus-evoked fluorescence changes, with yellow-to-red regions representing depolarization and blue-indigo regions corresponding to the baseline resting fluorescence (color scale right). By comparing the activity map with the resting fluorescence one can see that responses arise from cell bodies in the hilus as well as processes in

the inner molecular layer. Note that arrowheads 5 and 6 point to neurons that barely responded to PP stimulation. These same neurons responded strongly to GCL stimulation. **B.** Traces of fluorescence versus time from the numbered locations show downward-going depolarizations in response to PP stimulation (at the dashed grey vertical lines). **C.** As in **A** with the same field of view, but with stimulation of the GCL (75 μA); the same 6 MCs are highlighted. The response intensity map to the right and traces in **D** indicate they all 6 highlighted MCs responded robustly. The stimulating electrode is visible in the middle of the GCL in the resting fluorescence images. **D.** Traces of fluorescence versus time from the same locations as in **B**.

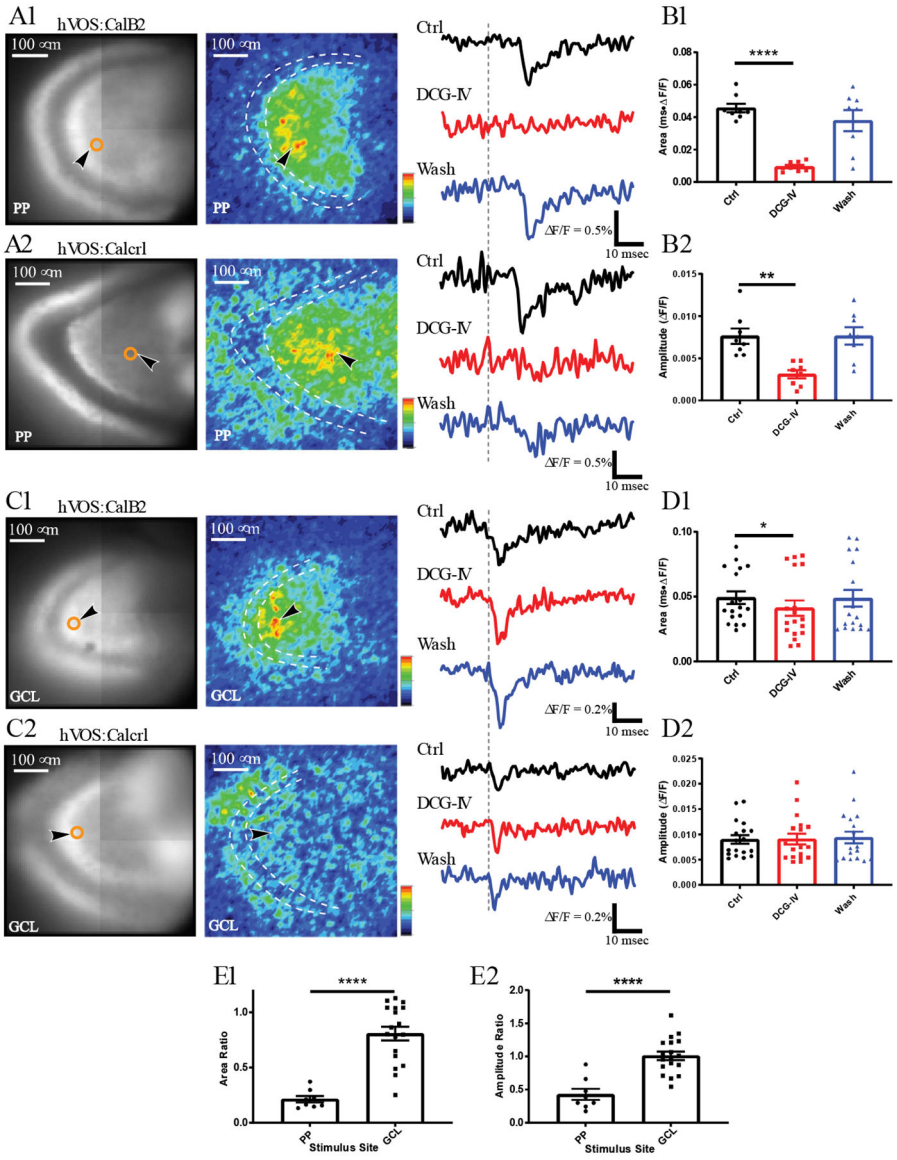

Figure 3.

Responses of MCs in slices from hVOS::CalB2 and hVOS::Calcrl mice. **A**.Resting fluorescence with the location of an MC (as in Figs. 2A and 2C – center) and response intensity maps 5–25 msec after stimulation (as in Fig. 2A and 2C – right) from an hVOS::CalB2 slice (A1) and an hVOS::Calcrl slice (A2). The dashed white contour outlines the GCL and black arrowheads point to neurons selected for trace display on the right. The PP was stimulated (200 μA) at times marked by vertical gray dashed lines. Traces display responses before (black), during (red), and after (blue) application of DCG-IV (1 μM). DCG-IV blocked responses in both hVOS::CalB2 and hVOS::Calcrl slices. **B**. Bar graph of response (mean ± SE), and individual MC responses as points. B1, Area under the curve: B2 Amplitudes. DCG-IV significantly decreased the area under the curve of MC responses evoked by PP stimulation (8 neurons, 3 slices, 3 hVOS::CalB2 animals, repeated measures one-way ANOVA, $p = 0.0011$ and 0.0008, Control vs. DCG-IV $p < 0.0001$ and $p = 0.0036$).

C. Resting fluorescence and response intensity maps of hVOS::CalB2 and hVOS::Calcrl slices as in **A**, but with stimulation in the GCL (200 μA and 50 μA, respectively). Traces on the right show MC responses before, during, and after DCG-IV application. Depolarizations in slices from both mouse lines were slightly reduced by DCG-IV. **D**. Bar graphs show that DCG-IV produced a small but significant decrease in the mean area under the curve of MC responses to GCL stimulation (D1), but not in amplitude (18 neurons, 7 slices, 7 hVOS::CalB2 animals; repeated measures one-way ANOVA $p = 0.024$; $p = 0.029$ for control vs. DCG-IV in **D1**). **E**. DCG-IV had a significantly smaller effect on GCL responses than on PP responses ($p < 0.0001$ for both **E1** and **E2**; *t*-test with Welch's correction). *, $p < 0.05$; **, $p<0.01$, ****, $p < 0.0001$.

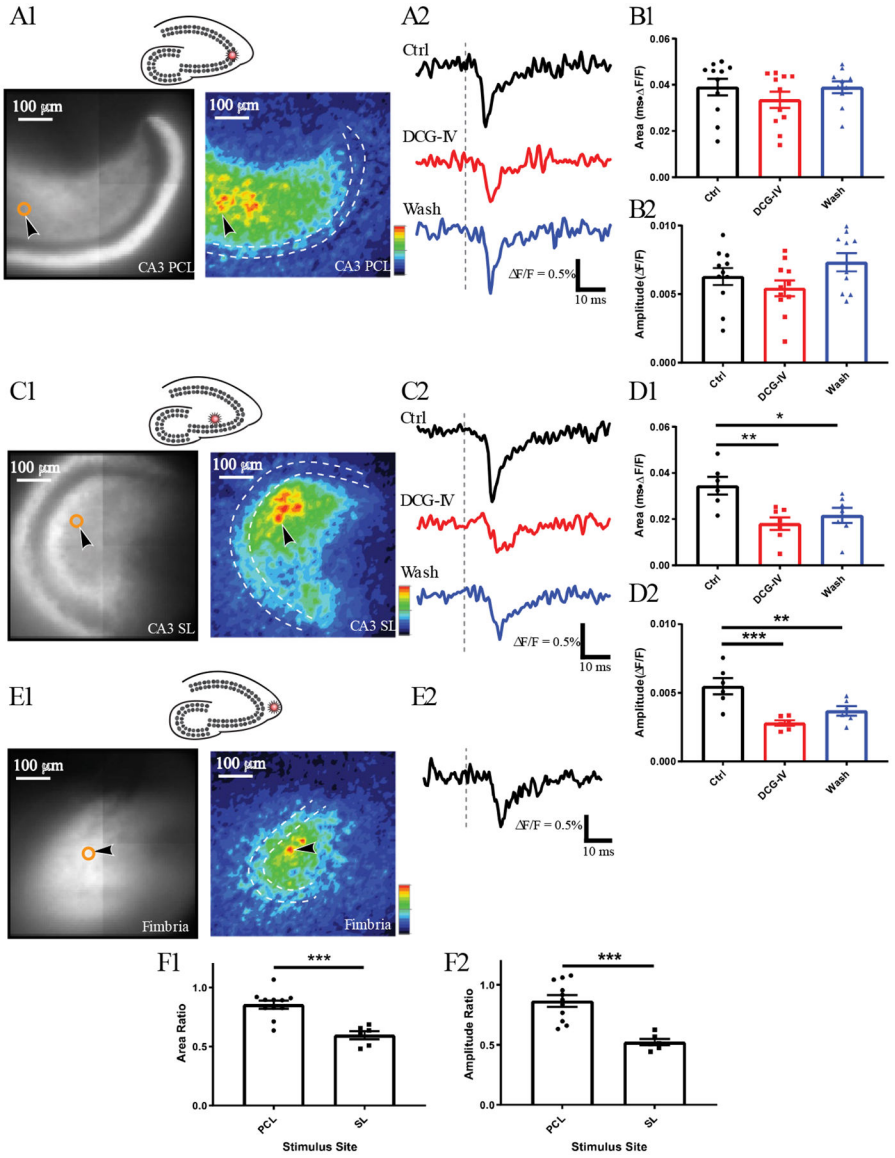

Figure 4.

hVOS imaging of MC responses to stimulation in the CA3 region. **A1**. Stimulation in the CA3 pyramidal cell layer (PCL, 100 μA), at the site marked by a star in the schematic above. Resting fluorescence and response intensity maps focus on the dentate gyrus, and the stimulation site is out of view. The dashed white contour outlines the GCL and the black arrowhead points to a neuron selected for trace display in **A2**. Traces of MC responses before (black), during (red), and after (blue) DCG-IV. Grey dashed lines indicate stimulation time. **B** Mean ± SE of response area (**B1)** and amplitude (**B2**) to PCL stimulation before, during and after DCG-IV. The weak blockade by DCG-IV was not statistically significant (11 neurons, 4 slices, 4 hVOS::CalB2 animals). **C1** Stimulation in the stratum lucidum (SL, 200 μA), at the site marked by a star in the schematic above. This is more likely to activate GCs antidromically. **C2.** Traces of MC responses before, during, and after DCG-IV show greater sensitivity than with PCL stimulation. **D**. Mean ± SE of area (**D1**) and amplitude

(**D2**) of responses to SL stimulation (7 neurons, 3 slices, 2 hVOS::CalB2 animals, one-way ANOVA p = 0.0072 and 0.0003, p = 0.005 and 0.0002 for Control vs. DCG-IV, p = 0.0251 and 0.0031 for Control vs. Wash). **E1**. Stimulation in the fimbria (200 μA), at the site indicated by the star in the schematic above. Stimulation of this site activates CA3 pyramidal cells antidromically. **E2**. An MC response shows a longer latency. **F**. DCG-IV had a greater effect on response area (**F1**) and amplitude (**F2**) to SL stimulation (11 neurons, 4 slices, 4 animals) compared to responses to PCL stimulation (6 neurons, 2 slices, 2 animals), and the differences were statistically significant (p = 0.0002 for both **F1** and **F2**; unpaired *t*-test). *, p < 0.05; **, p < 0.01; ***, p < 0.001.

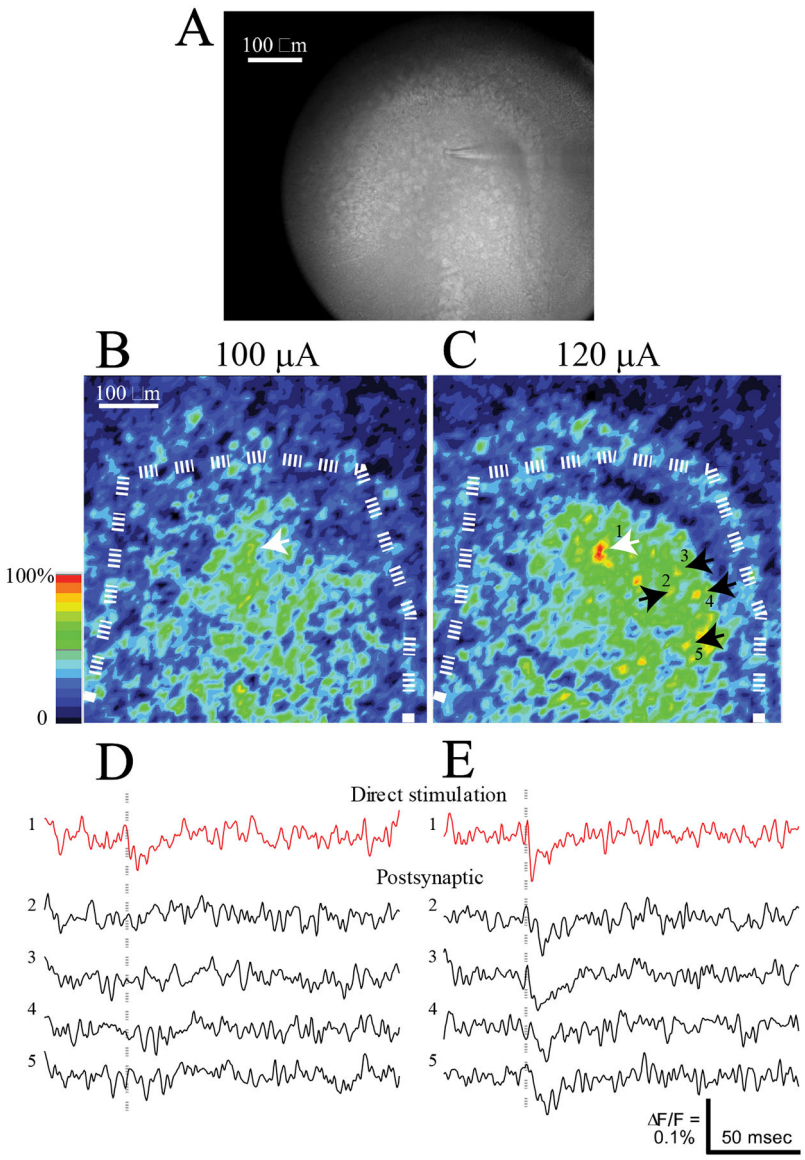

Figure 5.

Single MC stimulation. **A**. An IR-DIC image with a high-resolution camera shows a small-tipped theta glass electrode touching a MC directly beneath the tip. **B.** Response intensity map for a subthreshold stimulus (100 μA). A dashed white curve highlights the GCL. **C**. Response intensity map for a supra-threshold stimulus (120 μA). The white arrow indicates the cell directly stimulated by the electrode visible in **A**. Four black arrows and numbers indicate yellow spots representing depolarizations of postsynaptic cells. **D**. Fluorescence traces from the directly stimulated neuron (red) and four postsynaptic neurons (black) highlighted by arrows in **C** show that with a subthreshold stimulus only the directly simulated MC responded. Gray dashed lines indicate time of stimulation. **E**. Fluorescence traces from the same MCs in **D** to a supra-threshold stimulus. The response of the directly stimulated MC was larger and had a spike-like appearance. Responses with the shapes of synaptic potentials were seen in the four postsynaptic MCs.

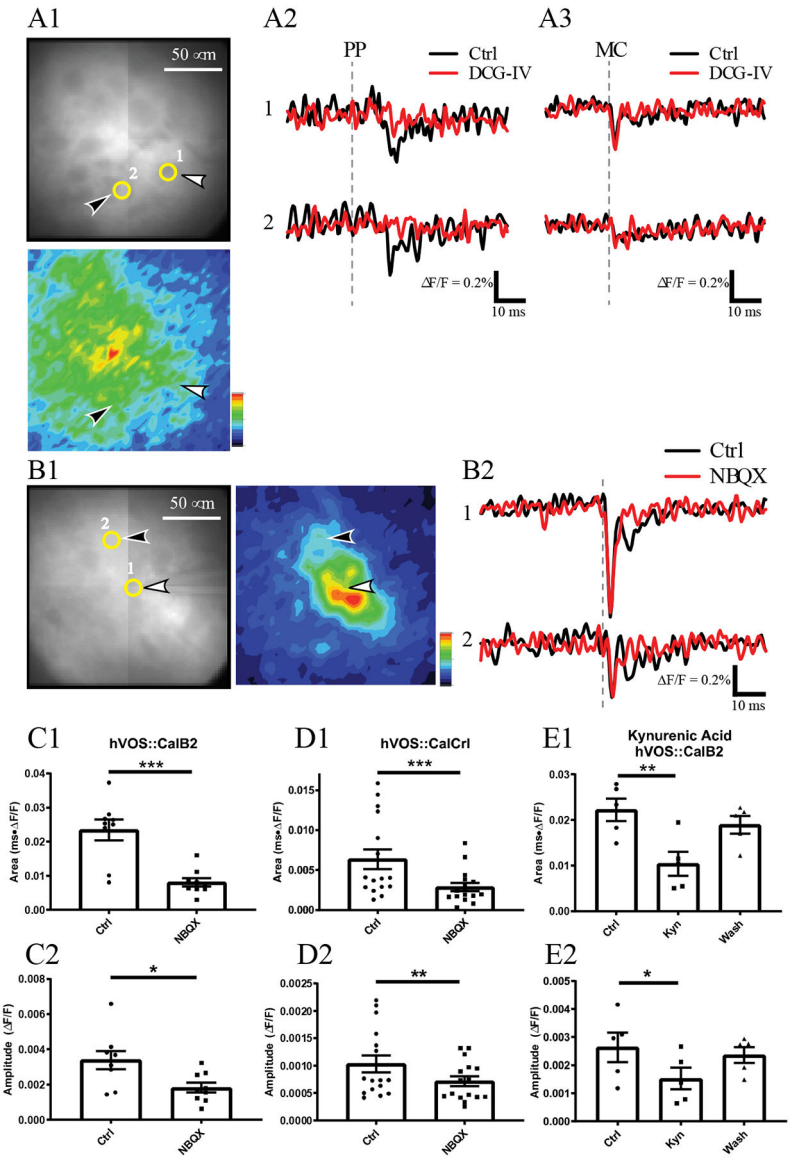

Figure 6.

Pharmacological sensitivity of MC responses to single MC stimulation. **A1**. Two MCs are indicated with numbers and yellow circles in the resting fluorescence image above, with white and black arrowheads pointing to the stimulated and unstimulated MCs, respectively. The response intensity map below (0–20 msec after theta electrode stimulation) shows that the targeted MC activates several MCs in this slice. Note that this image was taken with a higher magnification so the GCL is out of view. **A2**. Fluorescence traces show that PP stimulation (250 μA) depolarized the two highlighted MCs (black traces), and DCG-IV (red traces) blocked both of their responses. **A3**. Fluorescence traces show the responses to stimulation of neuron 1 with a theta electrode (200 μA). Neuron 1 produced an immediate spike and neuron 2 produced a synaptic response after a few miliseconds (black traces). Both responses were insensitive to DCG-IV (red traces). Grey dashed lines indicate time of stimulation. **B1**. An image of another experiment highlights two neurons, with resting

fluorescence left and response intensity map right. **B2**. Stimulation of neuron 1 with a theta electrode (300 μA) evoked a spike in neuron 1 as well as synaptic responses 5–10 msec after stimulation in both neurons (black traces). Application of NBQX (10 μM, red traces) blocked the synaptic responses but not the spike. Compiled drug actions. NBQX blocked responses in hVOS::CalB2 slices (9 neurons, 3 slices, 3 animals; paired *t*-test p = 0.0005 and 0.012 for **C1** and **C2**, respectively). NBQX blocked MC responses in hVOS::Calcrl slices (16 neurons, 6 slices, 3 animals; Wilcoxon matched-pairs signed rank test p = 0.0006 and 0.0063 for **D1** and **D2**, respectively). Kynurenic acid (Kyn, 1 mM) reversibly blocked MC response area, **E1**, and amplitude, **E2**, in hVOS::CalB2 slices (5 neurons, 3 slices, 3 animals; repeated measures one-way ANOVA p = 0.0003 and 0.021, p = 0.0026 and 0.015 for Control vs kynurenic acid). *, p<0.05; **, p < 0.01; ***, p < 0.001.

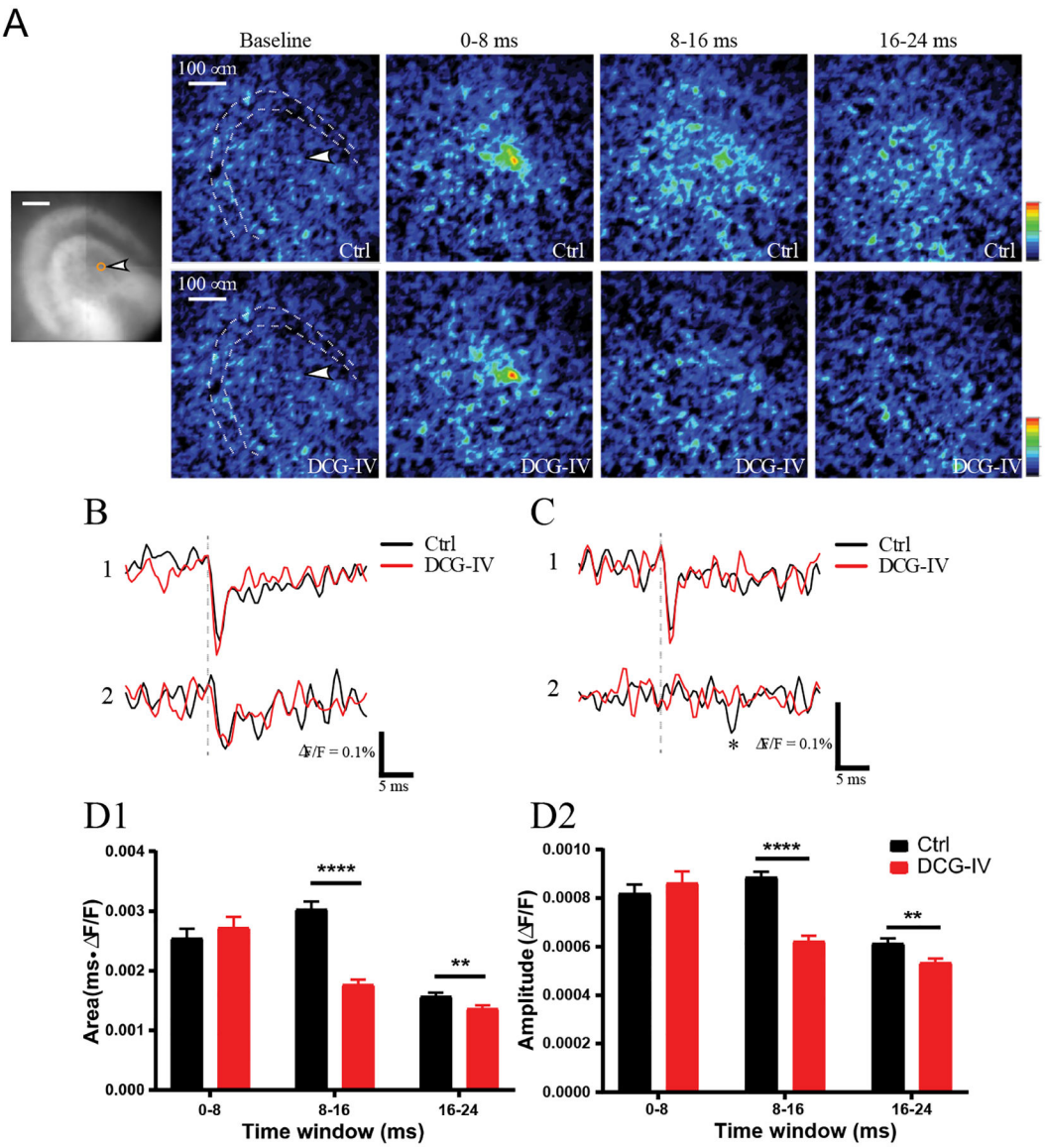

Figure 7.

Spread of responses to single MC stimulation. **A**. Response intensity maps in successive time windows before (to provide a baseline), 0–8 msec after, 8–16 msec after, and 16–24 msec after stimulation. The white arrowhead in the baseline window points to the stimulated MC. These maps illustrate the spatial distributions of responses to stimulation in control aCSF (above) and in DCG-IV (below). Note that DCG-IV block was much greater 8–16 msec after stimulation. **B.** Variable blockade of MC-MC signaling by DCG-IV. A DCG-IV insensitive response with a short latency. Direct stimulation of neuron 1 with a theta electrode produced an immediate spike and a short latency synaptic response in neuron 2. In both neurons, the control responses (black) were not blocked by DCG-IV (red). **C.** A similar experiment as in **B**, but with a long latency response in neuron 2, which was blocked by DCG-IV. **D**. Postsynaptic MC responses were separated into three latency windows and their sensitivity to DCG-IV evaluated. Responses before and after DCG-IV are shown in each

group. DCG-IV had no significant effect in the 0–8 msec group, a large highly significant effect in the 8–16 msec group, and a small significant effect in the 16–24 msec group (12 slices and 152 neurons from 3 hVOS::Calcrl mice; for **D1** and **D2**, respectively, Wilcoxon matched-pairs signed rank test $p = 0.0873$ and 0.399 for 0–8 msec, <0.0001 for 8–16 nsec, 0.0075 and 0.0037 for 16–24 msec). **, $p < 0.01$; ****, $p < 0.0001$.